Electron Spectroscopic Studies of CH_3OH Chemisorption on Cu_2O and ZnO Single-Crystal Surfaces: Methoxide Bonding and Reactivity Related to Methanol Synthesis

Paul M. Jones, Jennifer A. May, J. Brad Reitz, and Edward I. Solomon*

Contribution from the Department of Chemistry, Stanford University, Stanford, California 94305

Received November 18, 1996

Abstract: Adsorption of CH_3OH on $Cu_2O(111)$, ZnO(0001), and ZnO(10$\bar{1}$0) has been investigated with XPS, NEXAFS, variable-energy photoelectron spectroscopy (PES), and SCF-Xα Scattered Wave (SW) molecular orbital calculations. At high coverage (≥25.0L), CH_3OH is adsorbed as molecular multilayers on all three surfaces. At low temperatures (140 K) and coverage (0−0.6L), CH_3OH is deprotonated to form chemisorbed methoxide on all of the surfaces investigated. Under these conditions the C1s XPS peak positions are 289.5, 290.2, and 290.2 eV below the vacuum level, respectively. Annealing the $CH_3O^-/Cu_2O(111)$ surface complex to 523 K produces no other surface intermediate. Alternatively, at temperatures above 220 K on the ZnO-(0001) surface methoxide decomposes to produce a formate intermediate that is stable at the methanol synthesis reaction temperature (523 K). No formate surface intermediate is observed on the ZnO(10$\bar{1}$0) surface. The NEXAFS spectrum of chemisorbed methoxide on the $Cu_2O(111)$ surface exhibits a σ^* shape resonance at 294.8 eV giving a C−O bond length of 1.41 Å, a 0.02 Å contraction from the gas-phase methanol value. Methoxide chemisorbed on the ZnO(0001) surface is found to have a NEXAFS determined C−O bond length of 1.39 Å. These bond length contractions of the chemisorbed methoxide are due to the greater polarization of the C−O bond upon deprotonation and surface bonding. Variable-energy PES of the chemisorbed methoxide on $Cu_2O(111)$ gives a four peak valence band spectrum, with features at 20.0 (3a′), 15.6 (3a″, 5a″), 14.0 (σ_{CO}), and 10.0 eV (π_O, σ_O), below the vacuum level. SCF-Xα-SW molecular orbital calculations indicate that the bonding between the Cu(I) site and the CH_3O^- is dominated by the π_O, σ_O, and σ_{CO} levels, with a calculated σ charge donation from these levels into the empty Cu 4s and Cu $4p_z$ levels of 0.4e. As a consequence of deprotonation and σ donation the carbon atom in CH_3O^- is calculated to be 0.085e more positive than gas-phase methanol. The variable-energy PES of CH_3O^- on ZnO(0001) also exhibits four methoxide peaks, at 21.0 (5a′), 16.7 (2a″, 5a′), 13.6 (σ_{CO}), and 9.8 eV (π_O, σ_O). However, the σ donation is calculated to be less than half that found for CH_3O^- on the Cu(I) site (0.12e) and with 0.015 greater positive charge on the carbon atom, consistent with the relative binding energies of the C1s peaks and the greater C−O bond contraction. These results show that methoxide bonding to both Cu(I) and Zn(II) surface sites is dominated by σ donation. The electronic and geometric origins of the differences in bonding and reactivity among the Cu(I) and Zn(II) sites are addressed and provide insight into the molecular mechanism of the methanol synthesis reaction.

I. Introduction

The Methanol Synthesis Reaction (MSR) (eq 1) is an important industrial reaction, which in its modern form is catalyzed at low temperature (473−523 K) and pressure (50−100 atm) by the Cu/ZnO binary catalyst.[1,2] Before the availability of the binary catalysts, ZnO was used at higher reaction temperatures and pressures. The addition of copper to the ZnO catalyst greatly reduces the activation barrier for this reaction (eq 1) (from 30 kcal/mol to 18 kcal/mol).

$$CO + 2H_2 \xrightarrow{ZnO/Cu} CH_3OH \qquad (1)$$

Due to its industrial importance the binary catalyst has been extensively studied. Klier et al.[3−8] have shown that it contains a high affinity CO binding site that correlates with catalyst activity. Copper exists in the binary catalyst in several phases, including a dispersed metal phase and a smaller proportion of substitutional Cu(I) C_{3v} sites.[9−11] Didzulis et al.[12] have shown that these Cu(I) C_{3v} sites are the high affinity CO binding sites. The ICI group has utilized reactive frontal chromatography to show that the activity of the industrial catalyst also correlates

(1) Lee, S. *Methanol Synthesis Technology*; CRC Press: Boca Raton, FL, 1990; pp 1−22.
(2) Cheng, W. H.; Kung, H. H. *Methanol Production And Use*; Cheng, W. H., Kung, H. H., Eds.; Marcel Dekker: New York, 1994; pp 1−22.
(3) Bulko, J. B.; Herman, R. G.; Klier, K.; Simmons, G. W. *J. Phys. Chem.* **1979**, *83*, 3118.
(4) Dominquez, J. M.; Simmons, G. W.; Klier, K. *J. Mol. Catal.* **1983**, *20*, 369.
(5) Klier, K. *Adv. Catal.* **1982**, *31*, 243.
(6) Herman, R. G.; Klier, K.; Simmons, G. W.; Finn, B. P.; Bulko, J. B. *J. Catal.* **1979**, *56*, 407.
(7) Mehta, S.; Simmons, G. W.; Klier, K.; Herman, R. G. *J. Catal.* **1979**; *57*, 339.
(8) Klier, K.; Chatikavanij, V.; Herman, R. G.; Simmons, G. W. *J. Catal.* **1982**, *74*, 343
(9) Kau, L.; Hodgson, K. O.; Solomon, E. I. *J. Am. Chem. Soc.* **1989**, *111*, 7103.
(10) Kau, L.; Penner-Hahn, J. E.; Solomon, E. I.; Hodgson, K. O. *J. Phys. (Paris)* **1986**, *47*, C8−1177.
(11) Kau, L.; Spira-Solomon, D. J.; Penner-Hahn, J. E.; Hodgson, K. O.; Solomon, E. I. *J. Am. Chem. Soc.* **1987**, *109*, 6433.
(12) Didziulis, S. V.; Butcher, K. D.; Cohen, S. L.; Solomon, E. I. *J. Am. Chem. Soc.* **1989**, *111*, 7110.

S0002-7863(96)03990-X CCC: $15.00
Published on Web 02/03/1998

with the surface area of dispersed copper metal on the ZnO surface.[13−16] These conflicting observations remain of central concern in the study of the MSR reaction on the Cu/ZnO catalyst.

The methanol synthesis reaction, starting with CO, has been thought to proceed via a hydride transfer forming the formyl anion. The next reaction step, in this Costa−Muetterties reaction scheme, is likely the formation of formaldehyde or its isomer, which then abstracts another hydride to form the surface bound methoxide.[17−19] An alternate route to the formation of CH_3OH is the hydrogenation of carbon dioxide[1,5] given in eq 2.

$$CO_2 + 3H_2 \xrightarrow{Cu/ZnO} CH_3OH + H_2O \qquad (2)$$

CO_2 is added to the gas feedstock of the current MSR in a narrow range of partial pressures, which dramatically increases the rate of formation of CH_3OH.[20] Studies have shown that in the industrial application of the MSR CO_2 and not CO is the primary source of methanol.[21,22] However, the binary catalyst also catalyzes the water-gas shift reaction and thus complicates this result.[23] The hydrogenation of CO_2 over the binary catalyst proceeds via a formate intermediate, where the rate-limiting step in the formation of methanol is thought to be the breaking of the carbon−oxygen bond in the formate species.[16,24] In contrast, both Ren et al. and Klier[25,26] have shown that CO and not CO_2 is the primary source of methanol under the conditions studied. Thus the roles of CO and CO_2 and, Cu(I) and Cu(metal) in the MSR are still controversial.

ZnO has a wurtzite structure that contains tetrahedral zinc and oxide ions in the crystal structure. The Zn-terminated polar ZnO(0001) surface contains an outermost layer of coordinatively unsaturated Zn(II) sites with a next nearest layer of oxide anions, exposing both Lewis acid and Bronsted base sites. The ZnO-$(10\bar{1}0)$ surface is a nonpolar surface containing pairs of coordinatively unsaturated Zn(II) and oxide sites.[27,28] The direction of unsaturation of Zn(II) on this surface is tilted at 19° from the surface normal.[29,30] Cu_2O has a simple cubic structure where each oxide ion is surrounded by a tetrahedron of Cu(I) ions, and each Cu(I) ion is linearly coordinated to two oxide ions. The $Cu_2O(111)$ surface is a nonpolar surface possessing both coordinatively unsaturated oxide and cuprous ions at the surface.[31] Both ZnO and Cu_2O have filled 3d levels with localized metal and oxide bands in their photoelectron (PE) spectra. Their electronic structure, however, is considerably different, with the Zn 3d band centered at approximately 11.0 eV relative to the Fermi level which places it at approximately 5 eV deeper energy than the Cu 3d, owing to the greater effective nuclear charge on the Zn(II) metal ion.[31,32] This difference in d^{10} electronic structure is expected to contribute to differences in the interaction and surface chemistry of CH_3OH with these Zn(II) and Cu(I) surface sites.

Our previous studies of the surface chemistry of submonolayer Cu films on the chemically different ZnO crystal surfaces have shown that a coordinatively unsaturated Cu(I) C_{3v} site on the ZnO(0001) surface is the active center for the high affinity CO binding that has been correlated with high activity in methanol synthesis.[12] Cox et al.[33] have studied the Cu(I) site on the $Cu_2O(110)$ surface and shown that it binds CO with approximately the same heat of adsorption as the substitutional Cu(I) C_{3v} site, making it an attractive model of the Cu(I) high activity binding site possessing both metal ion and oxide surface sites. Kung et al.[34] have used the single-crystal surfaces of ZnO to probe the decomposition of CH_3OH; they showed that the ZnO(0001) surface is the dominant surface for this reaction where the main decomposition product was CO under the conditions of their experiment. The mechanism of methanol decomposition on the binary catalyst and ZnO has been extensively studied.[35−45] A formate surface species is thought to be a decomposition intermediate on both the binary catalyst and ZnO. Its relevance to the MSR relates to the CO_2 hydrogenation reaction[46,47] and its possible role in the water-gas shift reaction, where the binary catalyst is extremely effective in this reaction.

The emphasis of the current study is the systematic application of electron spectroscopies and molecular orbital calculations to probe the decomposition of methanol on single-crystal copper and zinc oxide surfaces and to use the results to obtain electronic structure insight into the methanol synthesis reaction. The contributions of surface specific geometric and electronic structures to reactivity are the central theme of this study. The XPS of the Cu_2O surface with increasing methanol exposure, studied at low temperatures to ensure the stability of any surface species, is presented in section III-A1. The temperature dependence of the methanol/$Cu_2O(111)$ surface complex is given in section III-A2, with the NEXAFS of this surface complex

(13) Denise, B.; Sneeden, R. P. A.; Beguin, B.; Cherifi, O. *Appl. Catal.* **1987**, *30*, 353.
(14) Chinchen, G. C.; Waugh, K. C.; Whan, D. A. *Appl. Catal.* **1986**, 25, 101.
(15) Chinchen, G. C.; Waugh, K. C. *J. Catal.* **1986**, *97*, 280.
(16) Chinchen, G. C.; Mansfield, K.; Spencer, M. S. *CHEMTECH* **1990**, *20*, 692.
(17) Costa, L. C. *Catal. Rev.-Sci. Eng.* **1983**, *25*, 325.
(18) Fahey, D. R. *J. Am. Chem. Soc.* **1981**, *103*, 136.
(19) Muetterties, E. L.; Stein, J. *Chem. Soc. Rev.* **1979**, *79*, 479.
(20) Lee, S. *Methanol Synthesis Technology*; CRC Press: Boca Raton, FL, 1990; pp 23−49.
(21) Kagan, Y. B.; Rozovskii, A. Y.; Lin, G. I.; Slivinskii, E. V.; Loktev, S. M.; Liberov, L. G.; Bashkirov, A. N. *Kinet. Katal.* **1975**, *16*, 704.
(22) Chinchen, G. C.; Denny, P. J.: Parker, D. G.; Spencer, M. S.; Whan, D. A. *Appl. Catal.* **1987**, *30*, 333.
(23) Satterfield, C. N. *Heterogeneous Catalysis In Practice*; McGraw-Hill: New York, 1980.
(24) Chinchen, G. C.; Spencer, M. S. *Catal. Today* **1991**, *10*, 293.
(25) Ren, Z.; Wang, J.; Lu, D. *Appl. Catal.* **1989**, *49*, 83.
(26) Vedage, G. A.; Pritchai, R.; Herman, R. G.; Klier, K. *Proceedings 8th International Congress On Catalysis*; Verlag Chemie: Berlin, 1984; Vol. 2, p 47.
(27) Gay, R. R.; Nodine, M. H.; Henrich, V. E.; Zeiger, H. J.; Solomon, E. I. *J. Am. Chem. Soc.* **1980**, *102*, 6752.
(28) Abrahams, S. C.; Bernstein, J. L. *Acta Crystallogr.; Sect. B* **1969**, *B25*, 1233.
(29) Duke, C. B.; Meyer, R. J.; Paton, A.; Mark, P. *Phys. Rev. B* **1978**, *18*, 4225.
(30) D'Amico, K. L.; Trenary, M.; Shinn, N. D.; Solomon, E. I.; McFeely, F. R. *J. Am. Chem. Soc.* **1982**, *104*, 5102.
(31) Lin, J.; May, J. A.; Didziulis, S. V.; Solomon, E. I. *J. Am. Chem. Soc.* **1992**, *114*, 4718.
(32) Lin, J.; Jones, P.; Guckert, J.; Solomon, E. I. *J. Am. Chem. Soc.* **1991**, *113*, 8312.
(33) Cox, D. F.; Schulz, K. H. *Surf. Sci.* **1991**, *249*, 138.
(34) Vest, M. A.; Lui, K. C.; Kung, H. H. *J. Catal.* **1989**, *120*, 231.
(35) Cheng, W. H.; Akhter, S.; Kung, H. H. *J. Catal.* **1983**, *82*, 341.
(36) Tawarah, K. M.; Hansen, R. S. *J. Catal.* **1984**, *87*, 305.
(37) Akhter, S.; Cheng, W. H.; Lui, K.; Kung, H. H. *J. Catal.* **1984**, *85*, 437.
(38) Edwards, J. F.; Schrader. G. L. *J. Phys. Chem.* **1984**, *88*, 5620.
(39) Akhter, S.; Lui, K.; Kung, H. H. *J. Phys. Chem.* **1985**, *89*, 1958.
(40) Tobin, J.; Hirschwald, W.; Cunningham, J. *Spectrochim. Acta* **1985**, *40B*, 725.
(41) Edwards, J. F.; Schrader, G. L. *J. Phys. Chem.* **1985**, *89*, 782.
(42) Chan, L.; Griffin, G. L. *Surf. Sci.* **1986**, *173*, 160.
(43) Vohs, J. M.; Barteau, M. A. *Surf. Sci.* **1986**, *176*, 91.
(44) Au, C. T.; Hirsch, W.; Hirschwald, W. *Surf. Sci.* **1989**, *221*, 113.
(45) Lazo, N. D.; Murray, D. K.; Kieke, M. L.; Haw, J. F. *J. Am. Chem. Soc.* **1992**, *114*, 8552.
(46) Bowker, M.; Houghton, H.; Waugh, K. C. *J. Chem. Soc., Faraday Trans. 1* **1981**, *77*, 3023.
(47) Bowker, M. *Vacuum* **1983**, *33*, 669.

presented in section III-A3. The UPS and variable-energy PES of the chemisorbed methoxide on the Cu_2O surface is correlated to the results of an SCF-Xα scattered wave SCF molecular orbital calculation in section III-A4. The XPS of ZnO exposed to methanol at low temperatures is presented in section III-B1. The temperature dependence of the surface complex is given in section III-B2. The NEXAFS of CH_3O^- on ZnO(0001) is presented in section III-B3. The UPS and variable-energy PES of methoxide on the ZnO(0001) surface at low temperature is correlated with the results of an SCF-Xα-SW calculation, in section III-B4. These results and their relevance to methanol synthesis are discussed in section IV.

II. Experimental Section

The Cu_2O(111) sample used in this study was a 1 mm thick single-crystal plate, oriented within 1° of the (111) direction by Laue backscattering and then polished with diamond grit until no pitting was visible under a low-power microscope. The oriented and polished crystal was then rinsed with hexane and acetone. Further cleaning in UHV was accomplished by using Ar ion sputtering in a series of sputter/anneal cycles at successively 2000, 1000, and 500 V accelerating voltage at 900 K followed by an anneal at this temperature. The oxidation state of copper was determined by using the X-ray induced Cu $L_2M_{4,5}M_{4,5}$ Auger peak. The surface cleanliness of the oriented crystal was checked with XPS spectroscopy.

The ZnO(0001) zinc terminated and the ZnO(10$\bar{1}$0) dimer surfaces used in this study were also 1 mm plates cut from single crystals and oriented to 1° by Laue backscattering and then polished with successively smaller sizes of diamond grit until no surface pits were observed. They were then etched with HCl and rinsed thoroughly with deionized water. These surfaces were further cleaned in a vacuum by Ar sputtering at successively 1000, and 500 V at 750 K, followed by annealing at this temperature. The cleanliness of these surfaces was checked by XPS spectroscopy.

Experiments using synchrotron radiation were performed at SPEAR III-1, VI-1, and X-1 beamlines at the Stanford Synchrotron Radiation Laboratory (SSRL) under dedicated operating conditions. For experiments in the VUV energy region a Grasshopper monochromator was used (beamline III-1). Spherical grating monochromators were used for experiments in the soft X-ray region (beamlines VI-1 and X-1). These beamlines have variable inlet and exit slits that allow a fixed monochromatic photon energy resolution to be maintained throughout the experiment: 0.2 eV for the Grasshopper and 0.5 eV for the spherical grating monochromators. A Perkin-Elmer Phi UHV system that had a double pass cylindrical mirror energy analyzer (CMA), ion sputtering gun, and a base pressure of 3×10^{-10} Torr was used for these experiments. For the studies performed on the Grasshopper monochromator the electron energy resolution of the CMA was maintained at 0.2 eV and for the soft X-ray studies the CMA resolution was set at 0.5 eV. Wider slits were used for the carbon kvv resolved NEXAFS measurements to increase the instrumental signal-to-noise. For the experiments reported here the incident synchrotron radiation was maintained at 75° with respect to the CMA central axis and thus impinged on the sample at close to a grazing angle. The photon flux was monitored by collecting the total electron yield from a high transmission grid freshly coated with gold via evaporation in the UHV system. All spectra were signal averaged until a sufficient signal-to-noise ratio had been attained. Clean background spectra were subtracted from the variable-energy valence band spectra of the surfaces with adspecies present. The resulting subtracted spectra were then fit with Gaussian/Lorentzian peaks by a curve-fitting procedure that varies their position, width, and height while minimizing the difference between the fit and experimental spectra. All spectra have been referenced to the vacuum level due to the effects of sample charging at the low temperatures used in this study.[48]

Both the Cu_2O and ZnO samples were heated and cooled in situ with the sample temperature measured with a Chromel-Alumel thermocouple directly attached to the sample holder. The CH_3OH used in this study was of analytic grade (99.9%) and was further purified by multiple freeze−pump−thaw cycles. All gases were introduced into the experimental chamber via a separate Varian leak valve attached to an independently pumped, gas manifold. All gas exposures were monitored with a nude ionization gauge.

The electronic structure calculations utilized the 1982 QCPE release of the SCF-Xα-SW program.[49−53] The atomic exchange parameter, α, was taken from Schwarz[54] and in the intersphere and outersphere regions the valence electron weighted average of the atomic α's was used. A Watson sphere was used for all ionic species and its radius was set at the outer sphere radius. All calculations were considered converged when the largest deviation of the atomic potentials between SCF cycles was less than 10^{-4} and was usually achieved in less than 300 cycles. Initial calculations were performed with the atomic radii chosen by the Norman criteria.[55] The accuracy of the calculated wave functions was determined by comparing the experimental PES valence band spectrum to that found by using the Slater transition state (TS) formalism.[56] It has been shown that the radii chosen with the Norman criteria overestimate ligand covalency for transition metal systems similar to those under investigation in this study.[57,58] Thus the sphere radii were systematically adjusted to fit the experimental data. All hydrogen atomic sphere radii were held constant at 1.0000 Bohr as suggested by Herman et al.[53] The Cu atomic radius was set at 2.9500 Bohr and the Zn atomic radius did not change from the Norman value (2.3295 Bohr).

Xα-SW molecular orbital calculations where performed on the surface complexes with and without the bound adspecies. These calculations were used to quantify the electron population changes with the addition of the adspecies and utilized the charge decomposed wave functions with full repartioning of the intersphere charge. All sphere radii used for this calculation (including the outer and Watson sphere) were identical.

III. Results and Analysis

A. Methanol Adsorption on Cu_2O(111). 1. XPS Studies of CH_3OH on Cu_2O(111). Figure 1A presents the C1s XPS spectra ($h\nu = 360$ eV) of a Cu_2O(111) single crystal surface exposed to increasing dosages (0.2L, 0.4L, 0.8L, 2.0L, 6.0L, 10.0L, and 25.0L) of methanol. These spectra exhibit a single broad peak, initially centered at an ionization potential (IP) of 289.5 ± 0.2 eV, which grows in intensity and width and gradually shifts toward higher energy with increasing surface coverage. The asymmetric growth of the C1s peak continues until a cumulative exposure of 25.0L. The C1s peak position for this coverage is 290.7 ± 0.2 eV, indicating that a shift of 1.2 ± 0.2 eV to higher energy has taken place with increased exposure. This high coverage, high energy peak is assigned to mutilayer physisorbed CH_3OH based on its energy position and standard literature values.[43,44]

2. Temperature Dependence of CH_3OH on Cu_2O(111). The multilayer CH_3OH on the Cu_2O(111) sample was stepwise heated to 180, 220, 273, and 523 K and monitored with C1s XPS. As shown in Figure 1B, an asymmetric attenuation of

(48) Watson, R. E.; Perlman, M. L.; Davenport, J. W. *Surf. Sci.* **1982**, *115*, 117.
(49) Slater, J. C. *Adv. Quantum Chem.* **1972**, *6*, 1.
(50) Johnson, K. H. *Adv. Quantum Chem.* **1973**, *7*, 143.
(51) Case, D. A. *Annu. Rev. Phys. Chem.* **1982**, *33*, 151.
(52) Connolly, J. W. D. *Semiempirical Methods of Electron Structure Calculation, Part A: Techniques*; Segal, G. A., Ed.; Plenum: New York; 1977.
(53) Herman, F.; Williams, A. R.; Johnson, K. H. *J. Chem. Phys.* **1974**, *61*, 3508.
(54) Schwarz, K. *Phys. Rev. B* **1972**, *5*, 2466.
(55) Norman, J. G. *Mol. Phys.* **1976**, *31*, 1191.
(56) Slater, J. C. *The Self-Consistent Field for Molecules and Solids: Quantum Theory of Molecules and Solids*; McGraw-Hill: New York; 1974; Vol. IV.
(57) Gewirth, A. A.; Cohen, S. L.; Schugar. H. J.; Solomon, E. I. *Inorg. Chem.* **1987**, *26*, 1133.
(58) Gewirth, A. A.; Solomon, E. I. *J. Am. Chem. Soc.* **1988**, *110*, 3811.

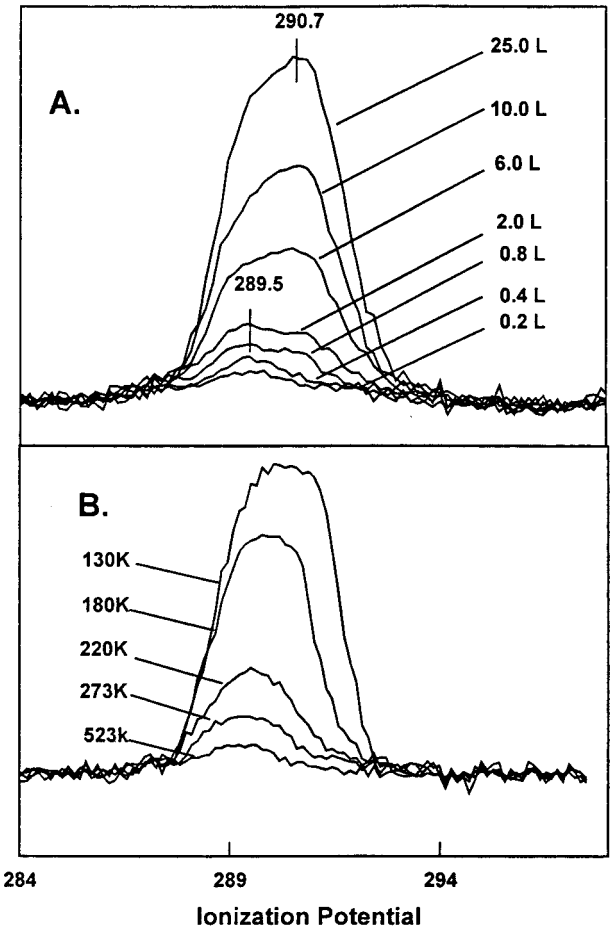

Figure 1. (A) The C1s XPS spectra of $Cu_2O(111)$ with increasing CH_3OH exposure. (B) The C1s XPS spectra of the stepwise heated multilayer on the $Cu_2O(111)$ surface incrementally heated to 180, 220, 273, and 523 K. Each heated spectrum was taken after a 60 s anneal at the indicated temperature and then cooled to 130 K for data acquisition. All spectra were taken with $h\nu = 360$ eV and were normalized to the incident flux.

the multilayer physisorbed peak is observed such that it shifts toward lower energy with increasing temperature. The C1s peak position of the annealed spectrum is 289.5 eV IP, indicating that both the low coverage, low temperature and high-temperature peak positions are the same and are thus associated with the same surface species. This surface species is assigned to chemisorbed methoxide based on its energy position and previous literature values.[43,44] No other surface species is seen on the $Cu_2O(111)$ surface from the decomposition of methanol up to 523 K. Parallel experiments were performed on the Cu_2O-(110) surface with identical results.

For comparison it is useful to estimate the energy position that molecular CH_3OH would have if it were chemisorbed to the surface. A relaxation correction to the C1s energy of gas-phase methanol was estimated by using the carbon kvv Auger energy of the methoxide surface species (261.0 ± 0.5 eV) and the shift, from gas phase, in its highest ionization energy valence band PES peak (-0.6 ± 0.1 eV).[59] This gives a molecular chemisorbed methanol energy of 287.6 ± 0.5 eV.[32,60] A comparison of this corrected energy position to that of the chemisorbed methoxide C1s peak position, at 289.5 ± 0.2 eV,

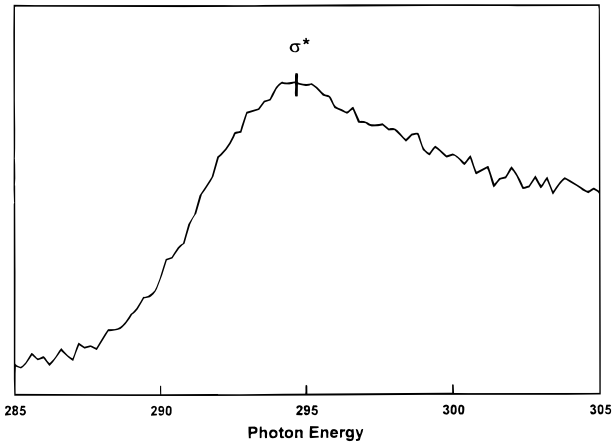

Figure 2. NEXAFS spectrum of methoxide/$Cu_2O(111)$. The spectrum was taken at 130 K and has been normalized to the incident flux. The methoxide covered spectrum was divided by a "low temperature clean" substrate spectrum taken with the same instrumental resolution.

shows that the methoxide is at approximately 2 eV higher energy. This relaxation corrected result indicates that the chemisorbed methoxide has a more positively charged carbon atom than found in gas-phase methanol.

3. NEXAFS of Low-Coverage CH_3OH on $Cu_2O(111)$. The carbon Auger yield NEXAFS spectrum of methoxide on $Cu_2O(111)$ is shown in Figure 2. A broad peak with a maximum centered at 294.8 ± 0.2 eV is observed and is ascribed to a σ^* shape resonance which is due to the scattering of the outgoing photoelectron by the interatomic potentials.[61] The energy position of this resonance is sensitive to the C−O bond length.[62,63] Stöhr et al.[64,65] have derived a semi-empirical expression that relates the energy separation, δ, between the C1s XPS (referenced to the Fermi level, see ref 48) position and the σ^* position to the C−O bond length for a series of surface bound molecules. δ is calculated to be 8.6 eV for methoxide chemisorbed to the $Cu_2O(111)$ surface. For comparison, the calculated δ for gas-phase CH_3OH, with a C−O bond length of 1.43 Å,[66] is 8.3 eV. The accuracy of this 0.3 eV shift between the experimental and calculated gas-phase value is dominated by the assignment of the σ^* peak position and is determined by the accuracy of the monochromator (± 0.2 eV) over the energy range of the transition. The C−O bond length for methoxide bound to the $Cu_2O(111)$ surface is estimated to be 1.41 Å. The intrinsic accuracy of this method (± 0.05 Å) is somewhat greater than the calculated change in bond length (-0.02 Å). However, δ has measurably increased, indicating that the C−O bond has shortened upon chemisorption to the $Cu_2O(111)$ surface.

(59) Seigbahn, K.; Nordling, C.; Johansson, G.; Hedman, J.; Heden, P. F.; Hamrin, K.; Gelius, U.; Bergmark, T.; Werme, L. O.; Manne, R.; Baer, Y. *ESCA Applied To Free Molecules*; North-Holland; Amsterdam-London, 1969.

(60) The total binding energy shift is given by $\Delta BE_{PES} = \Delta E - \Delta R_C$, where ΔE is the initial state chemical shift and the relaxation (ΔR_C) is derived from the energy shift in an Auger line. $\Delta KE_{AUGER} = -\Delta BE_V + 4\Delta R_V - \Delta R_C$, where R_v and R_c are related by the estimated size of the core and valence holes ($\Delta R_C/\Delta R_V = d_V/d_C$) and ΔBE_V is the binding energy shift in a nonbonding photoemission level. See ref 32.

(61) Dehmer, J. L.; Dill, D. J. *J. Chem. Phys.* **1976**, *65*, 5327.
(62) Stohr, J.; Jaeger, R. *Phys. Rev. B* **1982**, *26*, 4111.
(63) Stohr, J.; Gland, J. L.; Eberhardt, W.; Outka, D.; Madix, R. J.; Sette, F.; Koestner, R. J.; Doebler, U. *Phys. Rev. Lett.* **1983**, *51*, 2414.
(64) Stohr, J. *The Structure of Surfaces*; Van Hove, M. A., Tong, S. Y., Eds.; Springer-Verlag: Berlin, 1985.
(65) Stohr, J. *NEXAFS Spectroscopy*; Springer-Verlag: New York, 1992.
(66) Yarkony, D. R.; Schaefer, H. F., III; Rothenberg, S. *J. Am. Chem. Soc.* **1974**, *96*, 656.
(67) Wiberg, K. B. *J. Am. Chem. Soc.* **1990**, *112*, 3379.
(68) Liu, X.; Damo, C. P.; Lin, T. D.; Foster, S. C.; Misra, P.; Yu, L.; Miller, T. A. *J. Phys. Chem.* **1989**, *93*, 2266.
(69) Momse, T.; Endo, Y.; Hirota, E.; Shida, T. *J. Chem. Phys.* **1988**, *88*, 5338.

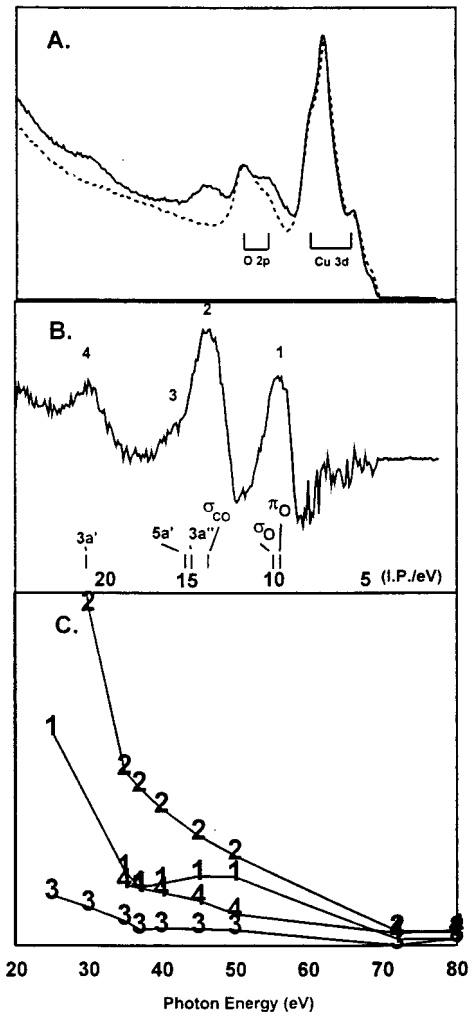

Figure 3. PE spectra of methoxide on $Cu_2O(111)$. (A) Clean Cu_2O-(111) spectrum (dashed line) along with the methoxide covered Cu_2O-(111) spectrum (solid line) taken with $h\nu = 40$ eV and normalized to the incident flux. These spectra have been aligned at the Cu 3d band. Both spectra were taken at a sample temperature of 130 K. The assignment of the PES peaks is included in the clean spectrum. (B) The difference spectrum (methoxide covered $Cu_2O(111)$ minus the clean $Cu_2O(111)$) showing the methoxide induced peaks labeled 1 through 4, along with the Xα TS methoxide valence orbital energy positions are indicated at the bottom of the figure. The deepest calculated transition has been aligned to peak 4. (C) The photon energy dependence of the four methoxide induced peaks on $Cu_2O(111)$.

Ab initio calculations have shown that the deprotonation of CH_3OH increases the polarization of the charge densities around the carbon and oxygen atoms thereby increasing their Coulombic attraction and contracting the C−O bond[66,67] (C−O in gas-phase CH_3O^- is 1.38 Å).[68,69]

4. Variable-Energy PES of $CH_3O^-/Cu_2O(111)$: Correlation With SCF-Xα-SW Molecular Orbital Calculations. To elucidate the electronic structure of the surface complex, valence band PES spectra of the chemisorbed methoxide on $Cu_2O(111)$ were collected and correlated to Xα-SW molecular orbital calculations. Shown in Figure 3A are the PES spectra of both clean $Cu_2O(111)$ and methoxide covered $Cu_2O(111)$ surfaces. The electronic structure of the clean Cu_2O surface (dashed line) has been extensively studied,[31,70−72] with the peak at 7 eV assigned as the Cu 3d band and the asymmetric band found between 9 and 13 eV as the oxygen 2p band. These spectra have been aligned and normalized to the Cu 3d band. No perturbation in the Cu 3d band is observed with the formation of the surface methoxide. Subtraction of the clean Cu_2O from the methoxide covered spectrum results in four methoxide related peaks, as shown in Figure 3B: peak 4 at 20.8 eV, peak 3 at 15.6 eV, peak 2 at 14.0 eV, and peak 1 at 10.0 eV.

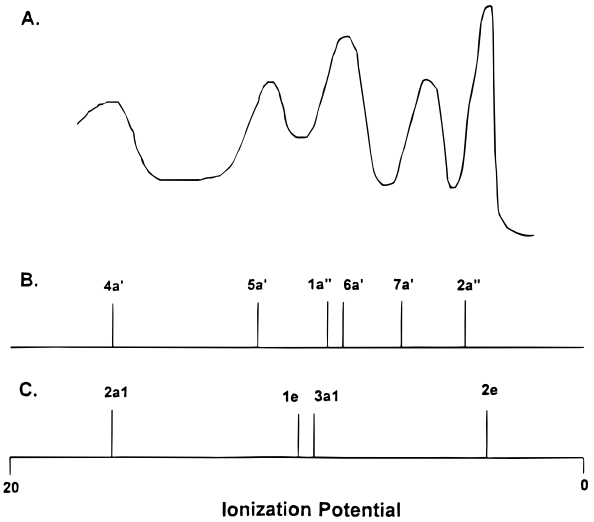

Figure 4. Comparison of the experimental He(II) PES of (A) gas-phase methanol (taken from ref 87) and (B) calculated Xα TS energy levels for gas-phase methanol. The gas-phase spectrum and calculation have been aligned at the deepest energy peak and the 4a′ transition. (C) The calculated methoxide transition state energy levels. The calculated result has been aligned by using the methanol 4a′ and the methoxide $2a_1$ levels.

Variable-energy photoelectron spectroscopy[73] was used to probe the bonding interactions between these methoxide levels and the Cu^+ site. Shown in Figure 3C are the integrated intensities of the four methoxide peaks and their variation with change in incident photon energy. The intensity of peak 1 decays rapidly after the ionization threshold and goes through a delayed maximum between 40 and 55 eV. This behavior indicates that peak 1 contains a Cu 3d component that has been mixed into the methoxide level, where the delayed maximum results from the centrifugal barrier in the radial Schrodinger equation for $l = 2$. Peak 2 displays higher intensity at threshold and some residual intensity through the 40−60 eV region.[74−78] Peaks 3 and 4 show little intensity after threshold and no delayed maximum.

Xα−SW calculations were performed and correlated to the PES data. Norman atomic sphere radii were initially used for these calculations. The transition state (TS) calculations were then adjusted by iteratively changing the sphere radii used in the SW solutions to more closely fit the PES spectrum. No change in spectral assignments was observed with the small changes in atomic sphere radii used (<0.3 Bohr). Calculations were first performed on gas-phase methanol and methoxide (pertinent bond lengths and angles used in this calculation are given in Supporting Information Table A). Shown in Figure 4A is the He(II) UPS spectrum of gas-phase methanol. The results of the Slater transition state (TS) calculations of methanol

(70) Wertheim, G. K.; Hufner, S. *Phys. Rev. Lett.* **1972**, *28*, 1028.
(71) Ghijsen, J.; Tjeng, L. H.; van Elp, J.; Eskes, H.; Westerink, J.; Sawatzky, G. A.; Czyzyk, M. T. *Phys. Rev. B* **1988**, *38*, 11322.
(72) Schulz, K. H.; Cox, D. F. *Phys. Rev. B* **1991**, *43*, 1610.
(73) Green, J. *Acc. Chem. Res.***1994**, *27*, 131.
(74) Fano, U.; Cooper, J. W. *Rev. Mod. Phys.* **1968**, *40*, 441.
(75) Eastman, D. E.; Kuznietz, M. *J. Appl. Phys.* **1971**, *42*, 1396.
(76) Manson, T. M.; Cooper, J. W. *Phys. Rev.* **1968**, *165*, 126.
(77) Cooper, J. W., *Phys. Rev.* **1962**, *128*, 618.
(78) Yeh, J. J.; Lindau, I. *At. Data Nucl. Data Tables* **1985**, *32*, 1−155.

Table 1. Xα Initial and Transition State Energies for CH_3O^-, Including the Orbital Charge Decomposition

CH_3O^-	initial state energy (eV)	transition state energy (eV)	C (% S,% P)	O (% S,% P)	% H
2e	4.56	8.68	(0.00, 3.96)	(0.00, 76.00)	15.00
$3a_1$	8.97	13.35	(0.00, 28.20)	(3.90, 59.15)	5.00
1e	9.83	14.04	(0.00, 48.00)	(0.00, 14.00)	39.00
$2a_1$	14.98	19.23	(41.65, 6.37)	(15.75, 4.83)	32.00

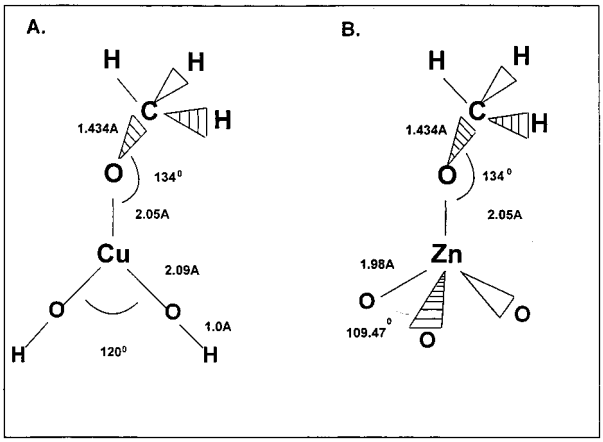

Figure 5. The geometry of the molecular clusters used for calculating the electronic structure of methoxide/Cu_2O(111) and methoxide/ZnO-(0001) sites. (A) The Cu^+ site was modeled with a bent C_{2v} HO−Cu−OH structure. (B) The Zn^{2+} surface site is approximated by a C_{3v} ZnO_3^{4-} molecular cluster. Pertinent bond lengths and angles are included in the figure.

are given in Figure 4B, where the calculation has been aligned to the deepest energy peak in the spectrum. An excellent overall fit of the calculated methanol spectrum to the experimental data is observed. A methoxide TS calculation was next performed by using these sphere radii. The charge decomposition calculated for the free methoxide is given in Table 1, and the transition state energy levels are shown in Figure 4C aligned to the methanol 4a′ peak. From the Xα results the lowest energy level (2e) is assigned to the oxygen $2p_{x,y}$ lone pair orbitals which split in energy upon binding the proton in CH_3OH. The next level to deeper binding energy is predominately an O $2p_z$ orbital which is σ bonding to the carbon ($3a_1$). The 1e and $2a_1$ levels both involve carbon−hydrogen bonding interactions which are mainly localized on the carbon atom. The "collapse" of the methanol spectrum into a three-peak pattern, upon deprotonation on an oxygen pre-dosed Cu surface, has been elucidated by Bowker et al.[79] The preceding Xα analysis confirms that the mechanism of the collapse is the change from C_s to C_{3v} site symmetry, which accompanies deprotonation, and establishes the important electronic interactions for the consideration of the metal−methoxide bond. The charge of the carbon atom in methoxide was calculated to be 0.115e more positive than that of the carbon in methanol, with the hydrogens of the methyl group becoming 0.104e more negative. Both of these results are consistent with a rearrangement of charge upon deprotonation.[67]

These calculations were extended to model the methoxide−Cu_2O surface site. The molecular cluster geometry used for these calculations is shown in Figure 5A. Here the Cu_2O(111) surface site has been approximated by a bent $Cu(OH)_2$ cluster[80] with the Cu−O bond length (2.09 Å) taken from the Cu_2O crystal structure. The angle of the Cu−O−C bond with respect to the O−Cu−O plane (134°) and the Cu-methoxide bond length (2.05 Å) was set from known crystal structures of copper(I) alkoxide complexes.[81] The molecular coordinates and atomic sphere radii used for this calculation are given in Supporting Information Table B. Norman atomic sphere radii were initially used for this calculation. The TS results yielded a Cu 3d band−O 2p band splitting of approximately 1−2 eV less than the experimental and had an unreasonably high covalency (a known limitation of the Norman criteria for sphere size determination in transition metal systems). The atomic sphere radii were then systematically adjusted until the TS calculation of the Cu 3d band−O 2p band splitting and covalency were in better agreement with the experimental results. The sensitivity of the methoxide centered levels to small changes in both the Cu−methoxide and C−O bond lengths (±0.1 Å) was also investigated. The amount of Cu character in the lower energy transitions increased 2−3% with a 0.1 Å shortening of the Cu−methoxide bond (a 2−3% decrease was observed for a 0.1 Å bond lengthening) and there was no significant change in the relative energy positions of these transitions. No change in covalency or energy position was observed with the small changes in C−O bond length (±0.1 Å). Thus the literature derived bond lengths are used in the study presented. The methoxide centered transitions derived from these calculations are shown at the bottom of Figure 3B. The calculated transitions have been aligned to peak 4 of the difference spectrum and exhibit an excellent overall fit to the data. Given in Table 2 are the calculated charge decompositions of the bound methoxide orbitals.

Table 2. Comparison of Xα Methoxide Centered Energy Levels of $Cu(OH)_2/CH_3O^-$ and $Zn(O)_3/CH_3O^-$, Including Initial State (IS), Transition State (TS) Energies, and Orbital Charge Decomposition

level	IS energy (eV)	TS energy (eV)	% C	% O	% H	% Cu 3d	% Cu 4s	% Cu 4p
				$Cu(OH)_2/CH_3O^-$				
$6a''/(\pi_O)$	3.35	5.96	6.00	60.00	8.00	11.20	0.00	1.60
$9a'/(\sigma_O)$	3.81	6.52	7.00	58.00	8.00	16.30	2.80	4.50
$6a'/(\sigma_{CO})$	7.95	11.03	29.00	53.00	6.00	4.20	2.00	3.90
3a″	8.35	11.63	48.00	13.00	36.00	1.40	0.70	1.60
5a′	8.44	11.70	51.00	8.00	40.00	0.00	0.00	0.00
3a′	14.08	17.56	50.00	19.00	27.00	1.20	0.90	1.20

level	IS energy (eV)	TS energy (eV)	% C	% O	% H	% Zn 3d	% Zn 4s	% Zn 4p
				$Zn(O)_3/CH_3O^-$				
$5a''/(\pi_O)$	5.62	8.54	4.00	83.00	7.00	2.00	0.00	1.00
$10a''/(\sigma_O)$	6.08	8.86	3.00	49.00	5.00	1.30	1.90	0.40
$4a'/(\sigma_{CO})$	10.11	13.13	28.00	51.00	6.00	11.20	1.70	1.10
2a″	10.92	14.27	48.00	7.00	44.00	0.60	0.20	0.20
6a′	11.03	14.41	48.00	6.00	46.00	0.00	0.00	0.00
5a′	16.72	19.95	50.00	17.00	32.00	0.40	0.20	0.30

The results of the Xα−SW calculation on the Cu^+ model active site indicate that peak 1 in the UPS spectrum is composed of two orbitals derived from the 2e level (oxygen $2p_x$ and p_y) of the methoxide which are split in energy due to differences in σ and π bonding with the metal at an Cu−O−C angle of 134° (Figure 5A) and is manifest in the data as a broadened peak. These methoxide centered orbitals, the 6a″ and the 9a′, have been labeled π_O and σ_O, respectively, in Table 2, underscoring their interaction with the Cu^+ binding site. Both

(79) Bowker, M.; Madix, R. J. *Surf. Sci.* **1980**, *27*, 190.
(80) Guckert, J. A.; Lowery, M. D.; Solomon, E. I. *J. Am. Chem. Soc.* **1994**, *117*, 2817.
(81) Osakada, K.; Takizawa, T.; Tanaka, M.; Yamamoto, T. *J. Organomet. Chem.* **1994**, *473*, 359.

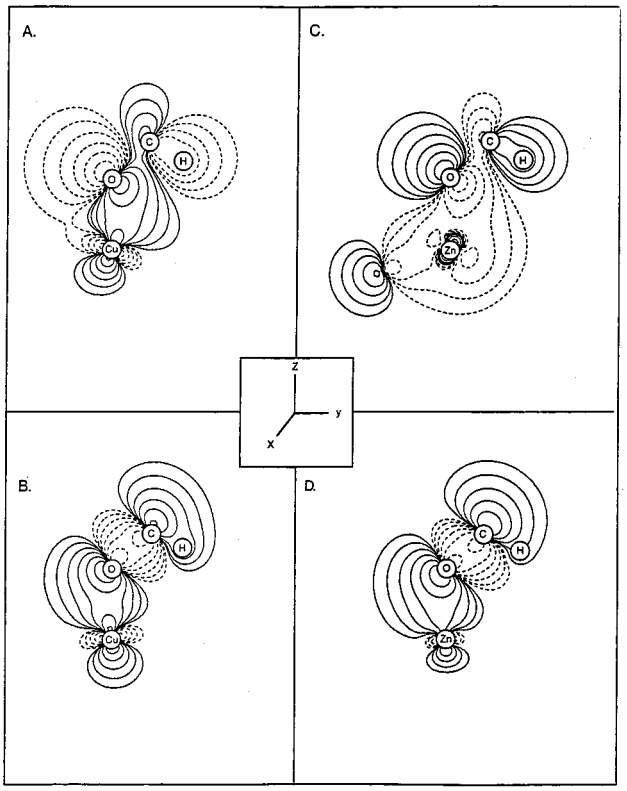

Figure 6. Xα scattered wave orbital contours of the σ_O and σ_{CO} methoxide levels on $Cu(OH)_2$ and ZnO_3. (A) 9a′ and (B) 6a′ of the $CH_3O^-/Cu(OH)_2$ molecular cluster. The (C) 10a′ and (D) 6a′ of the CH_3O^-/ZnO_3 cluster.

orbitals interact with the Cu 3d levels. The π_O orbital is perpendicular to the Cu−O−C plane and interacts with the Cu $3d_{xz}$ level; the calculation, in Table 2, indicates that approximately 11% Cu 3d is mixed into this level. Since both the π_O and Cu 3d levels are filled this interaction does not lead to net bonding between the methoxide and the Cu_2O surface.[32] The σ_O is in the Cu−O−C plane and interacts with the Cu^+ site through a σ-type interaction with the Cu d_{z^2}, 4s, and $4p_z$ levels. This interaction increases as the alkoxide fragment is rotated away from the surface normal.[82] The Xα charge decomposition indicates that at an angle of 134° there is 16.3% Cu $3d_{z^2}$ and 7.3% Cu 4s/4p character mixed into this methoxide centered level. Thus, the methoxide σ_O level has a significant bonding interaction with the unoccupied Cu 4s and 4p levels. The orbital contour of this level is shown in Figure 6A. The variable photon energy data for peak 1 shows a delayed maximum indicating a significant admixture of Cu 3d, consistent with the calculated 3d character in both π_O and σ_O levels (Figure 3C).

From Figure 3B and Table 2, peak 2 is assigned to the 6a′ methoxide centered orbital and is labeled σ_{CO} due to its σ-type interaction with the Cu^+ and has approximately 6% Cu4s/4p character. The orbital contour of this level is shown in Figure 6B. Peak 3 is due to the near overlap of the 3a″ and 5a′ orbitals, which have most of their electron density centered on the carbon atom and thus do not contribute to bonding with the Cu^+ site. Finally, peak 4 is assigned to the 3a′ orbital and has most of its electron density on the methyl group.

Of the six valence orbitals that comprise the chemisorbed methoxide PE spectrum, the above analysis shows that three levels dominate the bonding with the Cu^+ site: the π_O, σ_O, and σ_{CO}. Net bonding with the Cu^+ site involves charge donation from the methoxide σ_O and σ_{CO} levels into the unoccupied 4s and $4p_z$ levels of the Cu^+. To quantify these charge donations an electron population calculation was performed utilizing the Xα charge decomposition for both the C_{2v} $Cu(OH)_2$ model site and the site with bound methoxide (Table 3). Shown in the Δe column is the electron population change induced in each copper atomic orbital due to the methoxide bond. This calculation shows that the charge of the Cu $4p_z$ increases by 0.23e with the bonding of methoxide, whereas the 4s increases by 0.17e, thus reflecting the more effective overlap of the Cu $4p_z$ with the methoxide donor levels. The carbon in the bound methoxide is calculated to lose 0.085e compared to gas-phase methanol. This result is in accord with the chemical shift of the chemisorbed methoxide C1s peak and the NEXAFS determined C−O bond contraction. The hydrogens of the methyl group are calculated to become 0.04e more negative than gas-phase methanol. This result indicates that the methyl hydrogens have more hydride like character compared to gas-phase methanol.

Table 3. The Metal Ion Centered Electron Population of $Cu(OH)_2^{1-}$ and $(H_3CO)^-/Cu(OH)_2^{1-}$ and, $Zn(O)_3^{4-}$ and $(H_3CO)^-/Zn(O)_3^{4-}$, Including the Population Difference, Δ*e*, After Bonding CH_3O^-

orbital	$Cu(OH)_2^{1-}$	$(H_3CO)^-/Cu(OH)_2^{1-}$	Δe
Cu 4s	0.49	0.66	0.17
Cu $4p_x$	0.13	0.14	0.01
Cu $4p_y$	0.36	0.37	0.01
Cu $4p_z$	0.19	0.42	0.23
Cu $3d_{x^2-y^2}$	1.97	2.00	0.03
Cu $3d_{xz}$	2.03	2.03	0.00
Cu $3d_{z^2}$	2.09	2.11	0.02
Cu $3d_{yz}$	2.16	2.19	0.03
Cu $3d_{xy}$	2.08	2.07	−0.01
orbital	$Zn(O)_3^{4-}$	$(H_3CO)^-/Zn(O)_3^{4-}$	Δe
Zn 4s	0.64	0.72	0.08
Zn $4p_x$	0.37	0.39	0.02
Zn $4p_y$	0.37	0.39	0.02
Zn $4p_z$	0.15	0.21	0.04
Zn $3d_{x^2-y^2}$	2.08	2.05	−0.03
Zn $3d_{xz}$	2.03	2.04	0.01
Zn $3d_{z^2}$	1.99	1.98	−0.01
Zn $3d_{yz}$	2.03	2.03	0.00
Zn $3d_{xy}$	2.05	2.06	0.01

Thus methanol is deprotonated to form the surface bound methoxide species on Cu_2O at low coverage, low temperature, and high temperature. The C−O bond length in the bound methoxide is slightly contracted from the gas-phase methanol bond length by the increased polarization of the C−O bond which increases the net positive charge on the carbon atom and the net negative charge on the methyl hydrogens.

B. Methanol Adsorption on ZnO. 1. XPS Studies of CH_3OH on ZnO(10$\bar{1}$0) and ZnO(0001). The C1s XPS of the ZnO(10$\bar{1}$0) surface exposed to increasing dosages of methanol is presented in Figure 7A. An initial low coverage surface species is observed at 290.2 eV IP and can be assigned to chemisorbed methoxide due to its relationship to the previously presented chemisorbed peak on Cu_2O (vide supra) and literature values.[43,44] At high coverage a physisorbed methanol layer develops with an energy of 291.0 eV IP. For comparison Figure 8A gives the C1s XPS of a ZnO(0001) surface exposed to similar cumulative dosages of methanol. Consistent with the previous observation on the (10$\bar{1}$0) surface a symmetric peak at low exposures is observed with an IP of 290.2 eV and is likewise assigned to chemisorbed methoxide. At higher expo-

(82) Chisolm, M. H. *ACS Symp. Ser.* **1983**, 243.

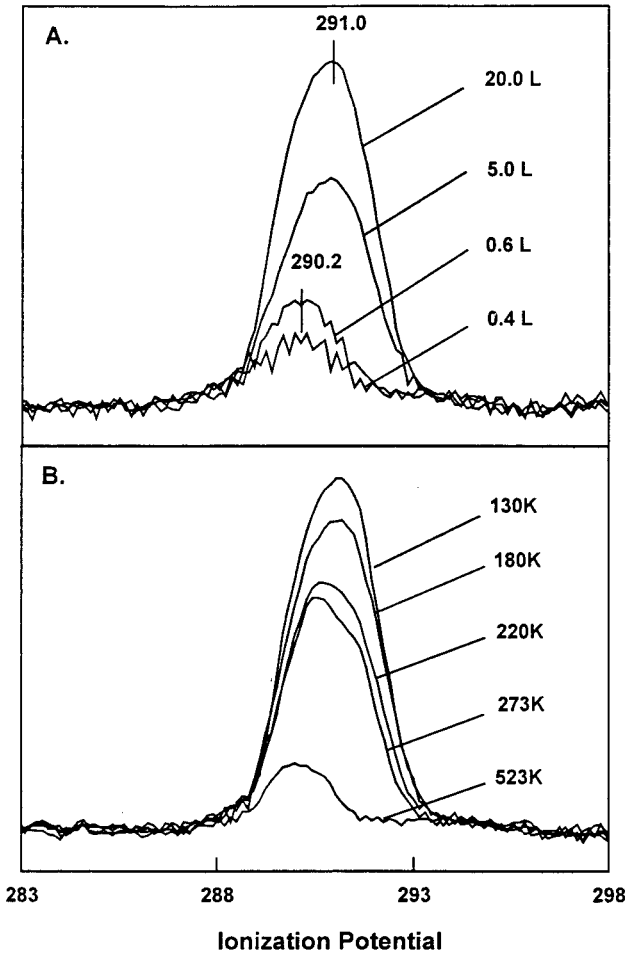

Figure 7. The C1s XPS spectra of (A) ZnO(10$\bar{1}$0) with increasing CH_3OH exposure. (B) The C1s XPS of multilayer CH_3OH on ZnO-(10$\bar{1}$0), incrementally heated to 180, 220, 273, and 523 K. Each heated spectrum was taken after a 60 s anneal at the indicated temperature and then cooled to 130 K for data acquisition All spectra were taken with $h\nu = 360$ eV and were normalized to the incident flux.

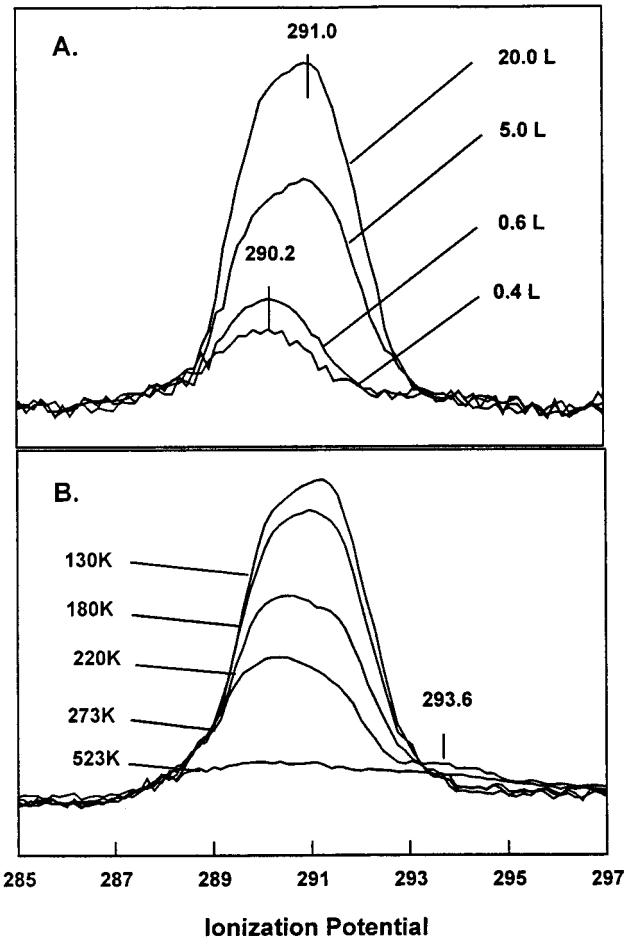

Figure 8. The C1s XPS spectra of (A) ZnO(0001) with increasing CH_3OH exposure. All spectra were taken with $h\nu = 360$ eV and were normalized to the incident flux. The sample temperature was maintained at 130 K. (B) The C1s XPS spectra of the stepwise heated multilayer CH_3OH on the ZnO(0001) surface annealed at 180, 220, 273, and 523 K. The formation of a high-temperature peak is indicated at 293.6 eV. Each heated spectrum was taken after a 60 s anneal at the indicated temperature and then cooled to 130 K for data acquisition. All spectra were taken with $h\nu = 360$ eV and were normalized to the incident flux.

sures a physisorbed CH_3OH multilayer develops (291.0 eV IP). These results indicate that the same low-temperature chemisorbed surface species (methoxide) is present on both ZnO surfaces.

2. Temperature Dependence of CH_3OH on ZnO(10$\bar{1}$0) and ZnO(0001). Shown in Figure 7B is the C1s XPS of the stepwise heated (180, 220, 273, and 523 K) CH_3OH multilayer on ZnO(10$\bar{1}$0). As was observed on the Cu_2O(111) surface, the physisorbed peak intensity seen at high coverage and low temperature drops with increasing temperature. A shift to 290.2 eV is observed with increasing temperature, indicating the presence of the same surface species at high and low temperature and coverage. Increasing the temperature further to 523 K decreases the intensity of the 290.2 eV peak. No other surface species are observed. The C1s XPS of the stepwise heated (180, 220, 273, and 523 K) CH_3OH multilayer on the ZnO(0001) surface shown in Figure 8B reveals the same shift to 290.2 eV IP of methoxide and the appearance of a new peak at 293.6 eV IP starting at 273 K. These peaks (290.2 and 293.6 eV), and thus their corresponding surface species, remain present to 523 K (Figure 8B), the low-temperature methanol synthesis reaction temperature. Barteau et al.[43] have observed a similar high-energy peak and assigned it to a surface bound formate. The above temperature-dependent behavior indicates that an additional surface reaction takes place at elevated temperatures (~273 K) on the (0001) surface.

3. NEXAFS of CH_3O^- on ZnO(0001). Shown in Figure 9 is the Auger yield NEXAFS spectrum of methoxide chemisorbed on the ZnO(0001) surface. A σ* shape resonance is observed at an energy of 295.5 eV. From the σ shape resonance position a δ of 9.3 eV is calculated, which is significantly larger than on Cu^+, and provides an estimated C−O bond length for methoxide on ZnO(0001) of 1.39 Å. Thus methoxide formed on the ZnO surface has a shorter C−O bond length compared to that of methoxide chemisorbed on Cu_2O.

4. Variable-Energy PES of CH_3O^- on ZnO(0001): Correlation with SCF Xα-SW SCF Molecular Orbital Calculations. As with CH_3O^- on Cu_2O, PES correlated with Xα-SW molecular orbital calculations were used to elucidate the electronic contributions to the bonding of methoxide on the ZnO surface. Figure 10A shows the PE spectrum ($h\nu = 50$ eV) of the low coverage methoxide on ZnO(0001) at 130 K, together with the spectrum of the clean ZnO(0001) surface taken under the same experimental conditions. The electronic structure of ZnO has been previously studied,[27,83] with the asymmetric peak

(83) Didzilius, S. V.; Cohen, S. L.; Butcher, K. D.; Solomon, E. I. *Inorg. Chem.* **1988**, *27*, 2238.

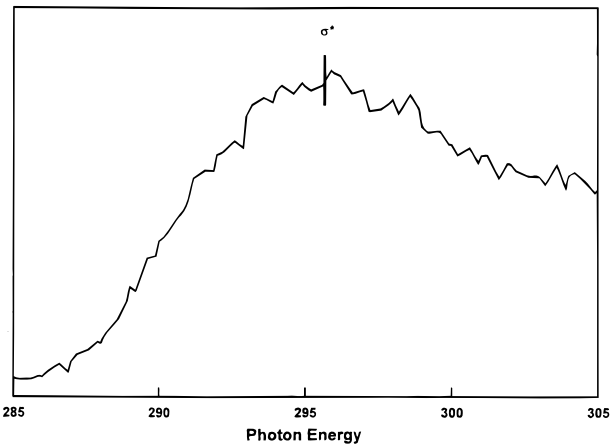

Figure 9. Methoxide/ZnO(0001) NEXAFS spectrum. The spectrum was taken at 130 K and has been normalized to the incident flux. The methoxide covered spectrum has been divided by a "low temperature clean" substrate spectrum taken with the same instrumental resolution.

located between 10 and 14 eV due to the oxygen 2p band and the peak at an ionization potential of 15 eV due to the Zn 3d band. These spectra are aligned and normalized to the Zn 3d band of the methoxide chemisorbed spectrum. Subtraction of the clean ZnO(0001) from the methoxide covered PES spectrum gives a four peak difference spectrum associated with methoxide chemisorbed on this surface (Figure 10B). Peak 1, at 9.8 eV, is at approximately 0.2 eV lower energy relative to peak 1 on the $Cu_2O(111)$ surface. Peak 2 at 13.6 eV is shifted to lower energy by 0.4 eV compared to the same peak on Cu_2O. Peak 3, at 16.7 eV, appears stabilized by 1.1 eV relative to the analogous peak for Cu_2O; however, this result is likely an artifact of the subtraction since this peak overlays the high energy side of the Zn 3d. Peak 4 at 21.0 eV has approximately the same energy as peak 4 on Cu_2O.

Variable-energy photoelectron spectroscopy was used to probe the atomic cross section components contributing to the peaks associated with the methoxide valence orbitals. Shown in Figure 10C is the integrated intensity of the four methoxide peaks as a function of photon energy. Peak 1 shows no intensity above the clean spectrum until approximately 40 eV photon energy and remains flat with increasing photon energy. This photon energy dependence is different from that of the same peak for the CH_3O^- on the $Cu_2O(111)$ surface, which exhibits a delayed maximum indicative of Cu 3d character. Peak 2 exhibits high intensity at low photon energy and goes through a delayed maximum between 40 and 60 eV, indicative of significant admixture of Zn 3d character[78] in this methoxide peak. The same methoxide peak on Cu_2O shows no delayed maximum (see Figure 3C). Peaks 3 and 4 show little intensity after ionization threshold and no delayed maximum.

Xα scattered wave calculations were performed to compare the electronic structure of methoxide chemisorbed on the ZnO surface relative to methoxide on Cu_2O. As shown in Figure 5B, a C_{3v} model of the Zn^{2+} binding site, with a Zn−O bond length of 1.98 Å, on the ZnO(0001) surface was used for this calculation.[84] The methoxide geometry used was the same as that for Cu_2O (the molecular coordinates and atomic sphere radii used are given in Supporting Information Table B). The atomic spheres used for this calculation were obtained by systematically adjusting the radii to give the best overall fit to the experimental Zn 3d−O 2p splitting (from 2 to 5 eV with adjusted spheres). Calculations were performed to assess the sensitivity of the

(84) Tossell, J. A. *Inorg. Chem.* **1977**, *16*, 2944.

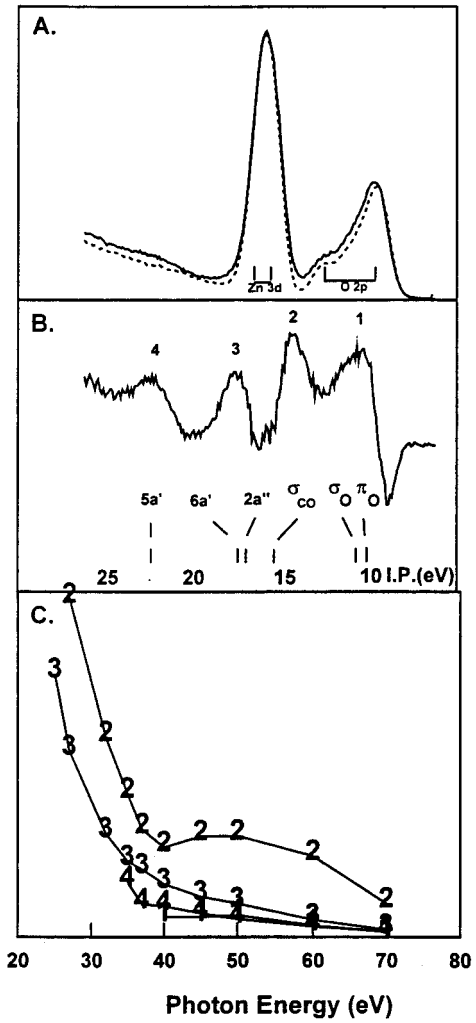

Figure 10. PE spectra of methoxide on ZnO(0001). (A) The spectra of the methoxide covered ZnO(0001) (solid line) and the clean ZnO-(0001) (dashed line) taken at 130 K and $h\nu = 50$ eV. The spectra have been normalized to the incident flux and aligned at the Zn 3d peak position. The assignment of the PES peaks is included in the clean spectra. (B) The difference spectrum (methoxide covered ZnO minus the clean ZnO) showing the methoxide induced peaks, labeled 1 through 4. The Xα TS positions are shown at the bottom of the figure and have been aligned to the deepest transition. (C) The photon energy dependence of the four methoxide induced peaks on ZnO(0001).

results to small changes in the Zn−methoxide bond (±0.1 Å). Only small changes in peak position or character were observed. Thus, as was the case for Cu_2O the literature derived bond length was used in the calculations presented. Superimposed in Figure 10B are the results of Slater transition state calculations for the Zn^{2+} model site, where only the methoxide centered levels are included for comparison to the difference PES peaks (no change in the spectral assignments of the methoxide levels was observed with the small changes in sphere radii used, <0.3 Bohr). A reasonable overall fit to the experimental methoxide peaks is observed. Table 2 gives the charge decomposition for these levels.

From the Xα TS energies, shown in Figure 10B, peak 1 is assigned to the near overlap of the π_O and the σ_O methoxide levels (vide supra). The π_O level, in contrast to CH_3O^- on Cu_2O, has little metal ion character (3.0% Zn), Table 2. The σ_O (the σ_O orbital contour is given in Figure 6C), however, has 2.3% Zn 4s/4p character and thus contributes to net bonding. In contrast to the CH_3O^- on Cu_2O, both the σ_O and the π_O levels possess very little Zn 3d character consistent with the

lack of a delayed maximum in the cross section in Figure 10C. Shown in Figure 6D is the orbital contour of peak 2, which is assigned to the σ_{CO} methoxide level and has 11.2% Zn 3d character, which is supported by the photon energy behavior of this peak (Figure 10C) showing a Zn 3d delayed maximum between 40 and 60 eV.[77] In contrast, the σ_{CO} peak on the Cu_2O surface has only 4% Cu 3d character. This large difference in 3d character is attributable to the closer proximity of the Zn 3d. In addition this level has 2.80% Zn 4s/4p (Table 3) that contributes to net bonding with the Zn^{2+}. Peak 3 is assigned to the overlap of the 6a′ and the 2a″ transitions, which are largely nonbonding with respect to the Zn^{2+}. Finally, peak 4 is assigned to the 5a′ level and is localized on the methoxide methyl group. These Xα results indicate that, as on Cu_2O, methoxide bonding to the Zn^{2+} site is dominated by three orbitals, the π_O, σ_O, and σ_{CO}, levels, with net bonding through the σ_O and σ_{CO} levels.

Table 3 gives the results of the calculated charge redistribution, Δe, upon methoxide bonding to ZnO. The electron population of both the Zn 4s and $4p_z$ increases with 0.08e being transferred to the Zn 4s orbital and 0.04e to the Zn $4p_z$. In comparison, the CH_3O^- bonding to the Cu^+ model site shows an increase of 0.17e and 0.23e respectively, indicating a larger charge transfer from the methoxide to the Cu^+ site. Thus, in parallel to the Cu^+ site, methoxide bonds to Zn^{2+} through the σ_O and σ_{CO} levels by σ donation into the 4s/4p levels. The extent of this donation is reduced by approximately 50% for Zn^{2+} versus Cu^+ surface sites.

The charge on the carbon and methyl hydrogens of methoxide bound to ZnO were calculated to be 0.100e more positive and 0.063e more negative, respectively, than methanol. Thus the carbon atom is 0.015e more positive and the hydrogens are 0.025e more negative than in methoxide chemisorbed to Cu_2O. The greater positive charge calculated for the carbon atom is consistent with the deeper binding energy of the C1s and the greater C−O bond contraction for CH_3O^- on ZnO.

Thus methanol is deprotonated on ZnO to form the surface bound methoxide at low coverage, low temperature and at temperatures up to 273 K. At temperatures above 273 K a formate intermediate is observed on the ZnO(0001), but not on the ZnO($10\bar{1}0$) surface, indicating that the additional reaction of methoxide is surface dependent. The C−O bond length of the bound methoxide is contracted from the gas-phase methanol value and is consistent with an increase in net positive charge on the carbon atom and net negative charge on the methyl hydrogens.

IV. Discussion

Methanol is deprotonated at low coverage and low temperature on both Cu_2O(111) and ZnO(0001) surfaces forming a surface bound methoxide. The deprotonation of methanol to methoxide on the Cu_2O(111) surface indicates that the exposed Cu^+ cations and oxide anions behave as Lewis acid and Bronsted conjugate base sites, respectively. The ZnO/methanol surface reaction has previously been calculated to proceed through an hydroxymethyl intermediate that, within the tight-binding approximation used, was shown to be more stable than the methoxy intermediate on the ZnO surface.[85] The surface formation of hydroxymethyl, if present, from deprotonation would be characterized by a C1s energy position lower than that of methanol due to reduced charge donation to a metal ion relative to hydrogen. The observation of a stable surface species (chemisorbed methoxide) whose relaxation corrected C1s energy position is at significantly deeper energy compared to methanol and with a measureably contracted C−O bond indicates that a hydroxymethyl intermediate is not formed on either the Cu_2O or ZnO surfaces.

Previous theoretical studies on gas-phase methoxide have shown that the carbon is more positively charged than in methanol, due to polarization of the C−O bond.[67] This is consistent with the presented Xα scattered wave calculations of methanol and methoxide which also show a polarization of the C−O bond with the carbon atom becoming more positively charged. This increased polarization leads to a contraction of the C−O bond. Xα scattered wave calculations of the model Cu^+ and Zn^{2+} surface methoxides also show a polarization of the C−O bond, with the carbon atom of the methoxide bound to Cu^+ having less positive charge compared to methoxide bound to the Zn^{2+} site. This is supported by the results of NEXAFS experiments where the contraction in the C−O bond is observed to be greater for methoxide chemisorbed to Zn^{2+} than Cu^+ due to the greater polarization of the bond on the Zn^{2+} surface site. The C1s XPS peak position also reflects this difference in polarization with the CH_3O^- on ZnO(0001) at 0.7 eV deeper energy than on Cu_2O(111), indicating a greater positive charge on the carbon atom of the Zn^{2+} surface complex. Using the repartioned atomic charges given in the Xα calculations an estimate can be made of the relative charge transfer between interacting atomic centers. For methanol this calculation yields approximately 0.8e transferred from the methoxide to the proton. This large charge transfer results in a large C−O bond polarization in methoxide due to the redistribution of charge which makes the hydrogens more negative and the carbon more positive when compared to methanol. In contrast, a similar calculation for the model methoxide−metal ion surface sites yields approximately 0.2−0.4e transferred from the methoxide to the metal ion. This smaller charge transfer results in a larger C−O bond polarization relative to methanol and hence bond contraction; however, the calculated polarization and thus bond contraction is less than that of gas-phase methoxide, as is observed experimentally.

Methoxide bound to Cu^+ and Zn^{2+} d^{10} surface sites behaves as a σ donor ligand, where the σ_O and σ_{CO} methoxide centered orbitals (Figure 6) dominate bonding by donating charge into the unoccupied 4s and 4p levels of the metal ion. This interaction is greatest for the Cu^+ site, with approximately twice the e^- donation than for the Zn^{2+} site. Furthermore, due to the proximity of the Zn 3d, d-character is at a maximum in the σ_{CO} level on the ZnO surface. This effect is opposite to that observed on the Cu_2O surface, where the d band is shifted to lower energy by approximately 7 eV due to the lower effective nuclear charge on Cu(I) and the d-character is largest for the σ_O level. This is supported by the difference in photoionization effects in Figure 3 versus Figure 10. However, since the d band is full this difference does not affect the net methoxide−metal ion bond. The effects of charge donation into the 4s and 4p orbitals on the surface bound methoxide are observed experimentally in the carbon charge and in the associated contraction of the C−O bond, where the Cu^+ site has the most σ donation and thus the longer C−O bond. For methoxide on the Zn^{2+} site the greater charge polarization and bond contraction imparts greater double bond character in the C−O bond and hydride character in the methyl hydrogens. This results in the methoxide bound to Zn^{2+} having formaldehyde-like character and a greater propensity for hydride donation to the surface (see resonance structures in Scheme 1).

The decomposition of methoxide takes place at high temperature on the ZnO(0001) surface to produce a formate

(85) Baetzold, R. C. *J. Phys. Chem.* **1985**, *89*, 4150.

Scheme 1

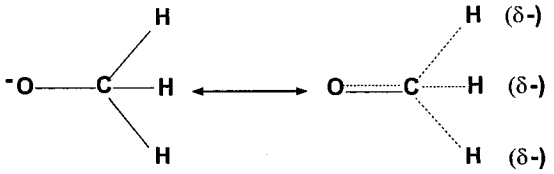

intermediate with an XPS peak at 293.6 eV. In contrast, no high temperature formate intermediate is observed on the Cu_2O-(111) site as a result of methoxide decomposition. These Zn-(II) versus Cu(I) surface dependent reactions can be related to the electronic structure differences between the surface metal ion−methoxide bonds. Kung et al.[37,46] have shown that the decomposition of methoxide proceeds through formaldehyde on ZnO. The electronic structure of the $CH_3O^--Zn^{2+}$ site which imparts formaldehyde like C−O bond and partial hydride character to the chemisorbed methoxide should facilitate the decomposition of methoxide by enabling hydride abstraction from methoxide by a neighboring Zn^{2+} site. In contrast, CH_3O^- chemisorbed on the $Cu_2O(111)$ surface has greater σ donor character which reduces the C−O and C−H bond polarization and thus does not facilitate the hydride abstraction necessary for the further decomposition of methoxide.

Both the ZnO(0001) and ZnO(10$\bar{1}$0) surfaces deprotonate methanol at low temperature and low coverage to form a chemisorbed methoxide. However, at high temperature the formate surface species is formed exclusively on the ZnO(0001) surface. Furthermore, recently completed studies on the interaction of formaldehyde on the ZnO(0001) and (10$\bar{1}$0) surfaces show that it is decomposed to formate on both of these ZnO surfaces.[86] Since the formaldehyde like character of the methoxide should be equivalent on the two ZnO surfaces studied, the high-temperature reactivity difference observed on these two surfaces should reflect structural differences which affect hydride abstraction. Using the methoxide geometry given in Figure 6B the distance between the methyl hydrogen and the next nearest Zn^{2+} is calculated to be 0.6 Å closer on the ZnO(0001) than the (10$\bar{1}$0) surface. Thus the facile abstraction of a hydride from the chemisorbed methoxide on the ZnO(0001) surface has at least two components: (1) the electronic structure, which results in more formaldehyde character in the surface intermediate, and (2) the specific surface geometry, which places a Lewis acid site in closer proximity to the methyl group of the methoxide for hydride abstraction.

The Methanol Synthesis Reaction (MSR) starting with bound carbon monoxide has previously been considered to proceed via the stepwise addition of hydrogen through a hydroxymethyl surface intermediate (Costa−Muetterties).[17−19] However, no such surface intermediate is formed from the decomposition of methanol on both Zn^{2+} and Cu^+ oxide model synthesis sites, where only the surface bound methoxide is observed. The electronic structure contribution to the reactivity of these two surface sites, which enhances the hydride character in the methyl hydrogens of the methoxide, supports a mechanism for the methanol synthesis reaction where the formaldehyde intermediate reacts via hydride attack from a Lewis acid site to produce methoxide. This reaction clearly takes place on the ZnO(0001) surface, which is consistent with previous single crystal studies showing that methanol decomposition dominantly occurs on the ZnO(0001) surface[37] and indicates that surface geometric as well as electronic structure contribute to this reactivity.

Acknowledgment. This research is supported by the NSF MRL program at the Center for Materials Research at Stanford University. Support for the work performed at the Stanford Synchrotron Radiation Laboratory, which is operated by the Department of Energy Division of Chemical Sciences, is gratefully acknowledged. The Authors also thank J. Guckert for assistance in data acquisition.

Supporting Information Available: Tables of geometric input parameters and Cartesian coordinates for SCF Xα SW calculations (2 pages). See any current masthead page for ordering and Internet access instructions.

JA963990Q

(86) Jones, P. M.; Reitz, B.; May, J.; Solomon, E. I. To be submitted for publication.

(87) Rubloff, G. W.; Luth, H.; Grobman, W. D. *Chem. Phys. Lett.* **1976**, *39*, 493.